Hindawi
Advances in Materials Science and Engineering
Volume 2018, Article ID 5750607, 11 pages
https://doi.org/10.1155/2018/5750607

Research Article

The Bending Responses of Sandwich Panels with Aluminium Honeycomb Core and CFRP Skins Used in Electric Vehicle Body

Yong Xiao,[1,2] Yefa Hu,[1,2] Jinguang Zhang,[1,2] Chunsheng Song,[1,2] Xiangyang Huang,[1,3] Jingui Yu,[1] and Zhaobing Liu[1,2]

[1]*School of Mechanical and Electronic Engineering, Wuhan University of Technology, Luoshi Road 122, Wuhan, Hubei 430070, China*
[2]*Institute of Advanced Materials Manufacturing Equipment and Technology, Wuhan University of Technology, Luoshi Road 122, Wuhan, Hubei 430070, China*
[3]*Fujian Hishan Machinery Co., Ltd., Hishan Road 666, Putian, Fujian 351100, China*

Correspondence should be addressed to Jinguang Zhang; cfrp204@163.com

Received 29 January 2018; Revised 31 May 2018; Accepted 19 June 2018; Published 7 August 2018

Academic Editor: Rujie He

Copyright © 2018 Yong Xiao et al. This is an open access article distributed under the Creative Commons Attribution License, which permits unrestricted use, distribution, and reproduction in any medium, provided the original work is properly cited.

The aim of this paper was to investigate bending responses of sandwich panels with aluminium honeycomb core and carbon fibre-reinforced plastic (CFRP) skins used in electric vehicle body subjected to quasistatic bending. The typical load-displacement curves, failure modes, and energy absorption are studied. The effects of fibre direction, stacking sequence, layer thickness, and loading velocity on the crashworthiness characteristics are discussed. The finite element analysis (FEA) results are compared with experimental measurements. It is observed that there are good agreements between the FEA and experimental results. Numerical simulations and experiment predict that the honeycomb sandwich panels with ±30° and ±45° fibre direction, asymmetrical stacking sequence (45°/−45°/45°/−45°), thicker panels (0.2 mm~0.4 mm), and smaller loading velocity (5 mm/min~30 mm/min) have better crashworthiness performance. The FEA prediction is also helpful in understanding the initiation and propagation of cracks within the honeycomb sandwich panels.

1. Introduction

Carbon fibre-reinforced plastic (CFRP) has been proven to be an effective energy absorbing material; it has been widely used in various industrial applications [1–8]. Moreover, the honeycomb filling has been shown to be efficient in improving the energy absorption characteristics of filling structures [9–16]. The honeycomb sandwich structures are widely used in several engineering applications in the transport industry.

There have been extensive studies regarding the impact and bending behaviour of aluminium honeycomb panels with and without external skins. Liu et al. [2] explored the crashworthiness of CFRP square tubes filled with aluminium honeycomb subjected to quasistatic axial crushing. By comparison, the peak load and absorbed energy of the filled tubes increased by more than 10% as compared with those of the bare CFRP tubes, ranging approximately from 12.41% to 27.22% and from 10.49% to 21.83%, respectively. For three-point bending (TPB), energy absorption (EA) and specific energy absorption (SEA) were found by Sun et al. [17] to be largely influenced by the structural parameters in the honeycomb core, but not much by the skin thickness. They also compared the crashworthiness of empty circular CFRP with CFRP/aluminium/steel tubes filled with aluminium foam or aluminium honeycomb under axial quasistatic crushing. With the increase in R of CFRP tubes, both the energy absorption and loading capacities increase, with specific energy absorption (SEA) increasing from 48.60 J/g to 60.37 J/g. The SEAs of CFRP tubes filled with honeycomb were slightly lower than the empty counterparts but far better than those of all metal specimens [18]. Hazizan et al. [19] investigated the low-velocity impact response of two glass fibre/epoxy aluminium honeycomb sandwich structures. Crupi et al. [20] investigated the mechanical behaviour under bending and impact loading of AHS panel reinforced by GFRP outer skins and a comparison with the

AHS panels (without GFRP skins) was done. The experimental tests demonstrated that the amount of energy absorption of the honeycomb sandwiches was highly improved, reinforcing them by means of GFRP outer skins. Hussein et al. [21] studied the axial crushing behaviour of aluminium honeycomb-filled square carbon fibre-reinforced plastic (CFRP) tubes. The results showed that the energy absorption (EA) of aluminium honeycomb-filled CFRP tubes increased from 20% to 36% more than the energy absorption of hollow CFRP tubes at different crushing velocities. Liu and Wu [22] investigated the lateral planar crushing and bending responses of CFRP square tubes filled with aluminium honeycomb. The results of lateral three-point bending tests showed that the peak load, EA, and SEA of honeycomb-filled CFRP tubes increased by 17%, 32%, and 0.9%, respectively, compared with the CFRP hollow tubes.

Although the honeycomb sandwich panels have been widely studied, there have been limited studies on the honeycomb sandwich panels with CFRP skins. Furthermore, it is a new attempt that the lightweight sandwich panels with aluminium honeycomb core and CFRP skins are applied to the body panel in our developed lightweight CFRP electric vehicle, which would be subject to lateral bending load. Therefore, their application requires a better understanding of the bending response of such lightweight composites, and most of the studies do not consider the material design of CFRP to improve bending performance.

2. Problem Definitions

2.1. The CAD Model of Sandwich Panels with Aluminium Honeycomb Core and CFRP Skins. The CAD model of sandwich panels with aluminium honeycomb core and CFRP skins is shown in Figure 1. It is made of two parts, known as upper and lower CFRP skins and middle aluminium honeycomb core. The CFRP skins are bonded to aluminium honeycomb core by DG-4 epoxy adhesive. The adhesive can be cured at room temperature and withstand temperatures from −60°C to +120°C. Moreover, the bonding process is simple, convenient to use and fast curing. The length and width of CFRP skins are 200 mm and 30 mm, respectively, and the thickness of CFRP skin is determined by layer thickness. The aluminium honeycomb core is made from the aluminium alloy with the cell thickness of 0.07 mm and side length of 4 mm. The height of aluminium honeycomb is 8.4 mm.

2.2. The Material Property of Sandwich Panels with Aluminium Honeycomb Core and CFRP Skins. Upper and lower CFRP skins are full carbon fibre structures, and their material is T700/FAW100. Table 1 lists the material properties of CFRP T700/FAW100. Nine material constants in Table 1 will be used in the finite element analysis.

The middle aluminium honeycomb core has an isotropic material property, and its material is 3003 aluminium alloy. The material properties are shown in Table 2.

2.3. Lay-Up Schemes of Sandwich Panels with Aluminium Honeycomb Core and CFRP Skins. In order to analyze the effect of stacking sequence, fibre direction, and layer thickness on the crashworthiness of sandwich panels, the specimens in this study are divided into three groups (Group A/Group B/Group C) as listed in Table 3. A total of eight different lay-up schemes (A/B/C/D/E/F/G) are considered. The fibre directions with 15°, 30°, 45°, 60°, and 75° are mainly considered. The purpose of Group A is to compare and analyze the effect of fibre direction on the crashworthiness of sandwich panels. The purpose of Group B is to compare and analyze the effect of stacking sequence on the crashworthiness of sandwich panels. The purpose of Group C is to compare and analyze the effect of layer thickness on the crashworthiness of sandwich panels.

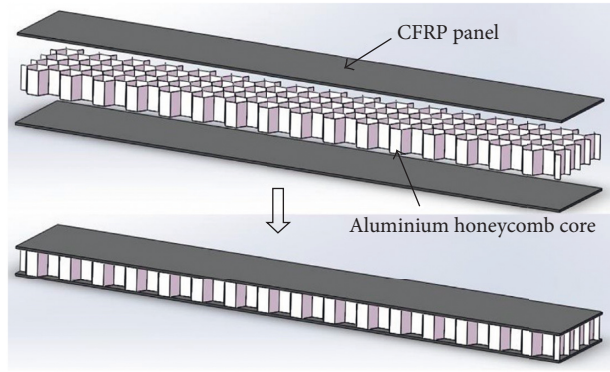

Figure 1: CAD model of sandwich panels with aluminium honeycomb core and CFRP skins.

2.4. Testing Methods. Different from the bending mechanical properties of conventional solid metal materials, the quasistatic three-point bending test is based on the GB/T1449-2005 Testing Standard "Test method for bending properties of carbon fiber reinforced plastics." As shown in Figure 2, the sandwich panel with aluminium honeycomb core and CFRP skins is placed parallel to the center position of the support seat of the universal testing machine. The loading roller moves downward at a constant rate of V until the specimen is broken. The load-displacement data are recorded during loading, and the experimental results of different cases are compared and analyzed.

3. Methods of Analyses

3.1. Orthotropic Material Property. Under the Cartesian coordinate 1-2-3, the constitutive equation of the orthotropic material such as carbon fibre-reinforced plastic is [22] as follows:

$$\begin{bmatrix} \sigma_{11} \\ \sigma_{22} \\ \sigma_{33} \\ \tau_{23} \\ \tau_{31} \\ \tau_{12} \end{bmatrix} = \begin{bmatrix} C_{11} & C_{12} & C_{13} & 0 & 0 & 0 \\ C_{21} & C_{22} & C_{23} & 0 & 0 & 0 \\ C_{31} & C_{32} & C_{33} & 0 & 0 & 0 \\ 0 & 0 & 0 & C_{44} & 0 & 0 \\ 0 & 0 & 0 & 0 & C_{55} & 0 \\ 0 & 0 & 0 & 0 & 0 & C_{66} \end{bmatrix} \begin{bmatrix} \varepsilon_{11} \\ \varepsilon_{22} \\ \varepsilon_{33} \\ \gamma_{23} \\ \gamma_{31} \\ \gamma_{12} \end{bmatrix}. \quad (1)$$

Table 1: The material properties of CFRP T700/FAW100.

E_1 (GPa)	E_2 (GPa)	E_3 (GPa)	ν_{21}	ν_{32}	ν_{31}	G_{12} (GPa)	G_{23} (GPa)	G_{13} (GPa)
150	9	9	0.24	0.24	0.28	5.12	5.12	3.34

E_1: longitudinal modulus, E_2, E_3: transverse modulus; ν_{21}: 21-direction Poisson's ratio, ν_{31}: 31-direction Poisson's ratio, ν_{32}: 32-direction Poisson's ratio; G_{12}, G_{13}: 12-direction, 13-direction shear modulus, G_{23}: 23-direction shear modulus.

Table 2: The material properties of the aluminium honeycomb core.

E (GPa)	ν	ρ (kg/m^3)	σs (Pa)
70	0.33	$2.70E+03$	$2.76E+07$

E: elastic modulus, ν: Poisson's ratio; ρ: density, σs: yield strength.

Table 3: Lay-up schemes of sandwich panels.

Case	Stacking
Group A	
A	[45°/−45°/45°/−45°]
B	[30°/−30°/30°/−30°]
C	[60°/−60°/60°/−60°]
D	[75°/−75°/75°/−75°]
E	[60°/−15°/15°/−60°]
Group B	
A	[45°/−45°/45°/−45°]
F	[45°/−45°/−45°/45°]
Group C	
A	[45°/−45°/45°/−45°]
G	[45°/−45°/45°]
H	[45°/−45°]

The abovementioned equation can be written in a simple form:

$$\{\sigma\} = [C]\{\varepsilon\}, \tag{2}$$

where $\{\sigma\}$, $\{\varepsilon\}$, and $[C]$ are the stress, strain, and stiffness matrix, respectively. The compliance matrix $[C]$ is the inverse of $[C]$ as follows:

$$[S] = [C]^{-1} = \begin{bmatrix} \frac{1}{E_1} & \frac{-\nu_{21}}{E_2} & \frac{-\nu_{31}}{E_3} & 0 & 0 & 0 \\ \frac{-\nu_{12}}{E_1} & \frac{1}{E_2} & \frac{-\nu_{32}}{E_3} & 0 & 0 & 0 \\ \frac{-\nu_{13}}{E_1} & \frac{-\nu_{23}}{E_2} & \frac{1}{E_3} & 0 & 0 & 0 \\ 0 & 0 & 0 & \frac{1}{G_{23}} & 0 & 0 \\ 0 & 0 & 0 & 0 & \frac{1}{G_{31}} & 0 \\ 0 & 0 & 0 & 0 & 0 & \frac{1}{G_{12}} \end{bmatrix}, \tag{3}$$

where E_i, G_{ij}, and ν_{ij} are Young's modulus, shear modulus, and Poisson's ratio, respectively. The symmetrical matrix $[S]$ in (3) has nine independent material constants for the orthotropic material.

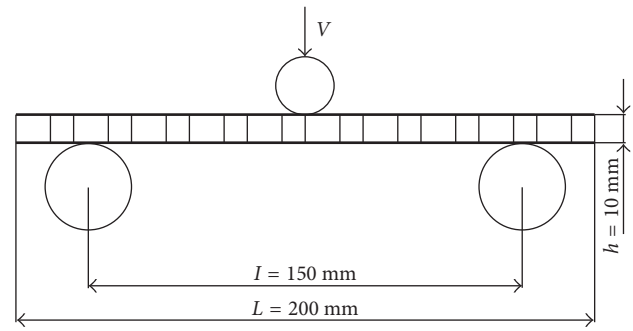

Figure 2: Schematic of quasistatic three-point bending test.

In the carbon/epoxy composite laminate, each ply has the orthotropic material property. The fibre directions of each ply can be different for practical applications. The bicycle frame is a full carbon fibre structure, and its material is T700/FAW100. Table 1 lists the material properties of CFRP T700/FAW100. Nine material constants in Table 1 will be used in the finite element analysis.

3.2. Finite Element Analysis (FEA). In this study, finite element analysis (FEA) is performed using ABAQUS software including model and mesh, load, boundary condition, solving, and postprocessing. Figure 3 shows the finite element model of sandwich panels with aluminium honeycomb core and CFRP skins. It is supported by a rigid support seat at the bottom. The rigid loading roller moving at a constant velocity was built to represent the loading for three-point bending. The sandwich panels necessitate a progressive failure model for solid elements using a modified Chang-Chang failure criterion, which is capable of predicting tensile and compressive fibre failure, as well as tensile and compressive matrix failure. The aluminium honeycomb is modelled by solid elements with isotropic material property. There are three types of contact defined between the loading roller, CFRP skins, aluminium honeycomb core, and support seat, namely, automatic single surface, tied surface to surface, and automatic nodes to surface (as illustrated in Figure 3). The loading speed and boundary conditions were prescribed consistently with the experimental setup.

3.3. Crashworthiness Criteria. To quantify the crashworthiness, several different criteria are often used, namely, initial peak force ($F_{\max}$), mean crushing force (MCF), crush force efficiency (CFE), energy absorption (EA), and specific energy absorption (SEA) [3].

The initial peak force ($F_{\max}$) can be obtained directly from the load-displacement curve which separates the

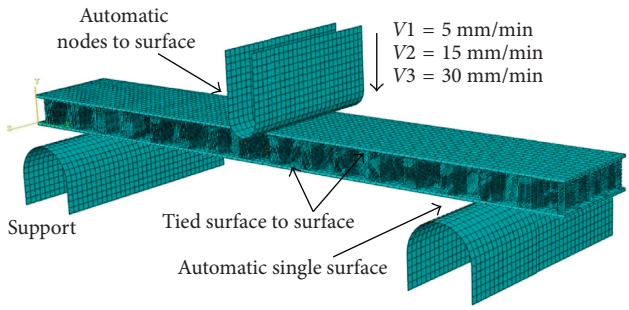

Figure 3: Schematic of finite element model.

loading process into the initial elastic bending stage and bending collapse stage.

The value of average crushing force (F_{avg}) is defined mathematically as

$$F_{avg} = \frac{1}{d}\int_0^d F(\delta)\,d\delta, \tag{4}$$

where d is the collapse distance and $F(\delta)$ is the instantaneous crush force.

Crush force efficiency (CFE), defined as the ratio of the mean crushing force (MCF) to the initial peak force (F_{max}), is used to measure the uniformity of crushing force as

$$\text{CFE} = \frac{F_{avg}}{F_{max}}. \tag{5}$$

The higher the value of CFE, the better the crashworthiness performance.

The energy absorption (EA) is obtained by integrating the load-displacement curve during the loading process as

$$\text{EA} = \int_0^d F(\delta)\,d\delta. \tag{6}$$

The higher the energy absorption (EA), the better the crashworthiness. To account for the effect of mass (weight), specific energy absorption (SEA), defined as

$$\text{SEA} = \frac{E_a}{m} = \frac{\int_0^d F(\delta)\,d\delta}{m}, \tag{7}$$

is frequently used as one of the most critical crashworthiness criteria.

4. Experimental Procedures

4.1. Specimen Preparation. For electric vehicles, the most effective way to increase the extension mileage is to reduce weight. The traditional materials of vehicle body are high-strength steel or aluminium alloys, which are heavy and do not meet the growing extensive mileage requirements of electric vehicles. The sandwich panels with aluminium honeycomb core and carbon fibre-reinforced plastic (CFRP) skins can be reasonably designed to make electric vehicle body with the advantages of lightweight and better energy absorption performance. As shown in Figure 4, the filled structures are applied to the typical structural elements such as the body panels in our developed lightweight CFRP

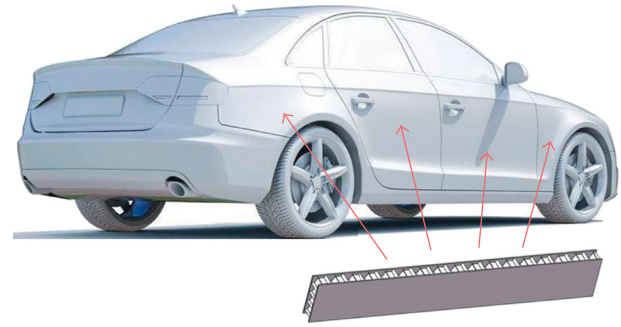

Figure 4: Schematic of sandwich structures with aluminium honeycomb core and CFRP skins in vehicle body.

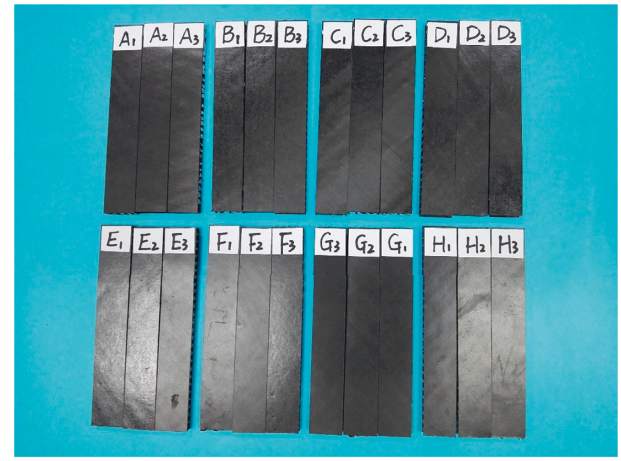

Figure 5: Specimens before quasistatic three-point bending test with different lay-up schemes.

Figure 6: Specimens before quasistatic three-point bending test with different loading speeds.

electric vehicle, which would be subject to lateral bending load. This work aimed at investigating the lateral bending capability of sandwich panels with aluminium honeycomb core and CFRP skins. Figure 5 shows the specimens of sandwich panels with eight different lay-up schemes. In order to analyze the effect of stacking sequence, fibre direction, and layer thickness on the crashworthiness of sandwich panels, a total of eight different lay-up schemes (A/B/C/D/E/F/G/H) are considered. To ensure the accuracy of the experimental results, each case is repeated three times

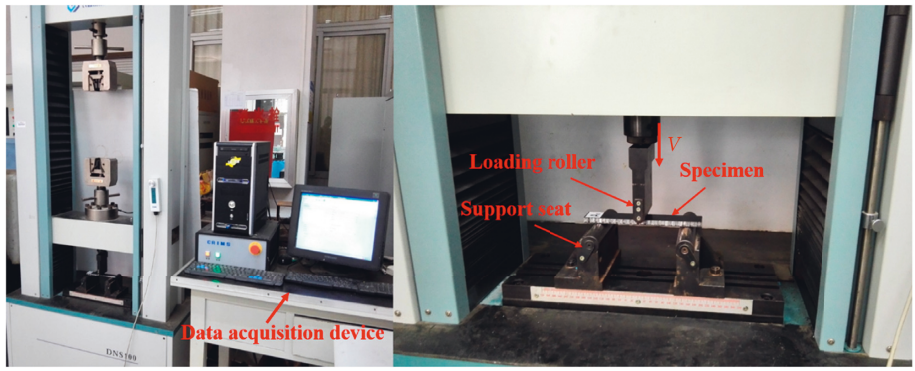

Figure 7: Specimens tested in the electronic universal testing machine.

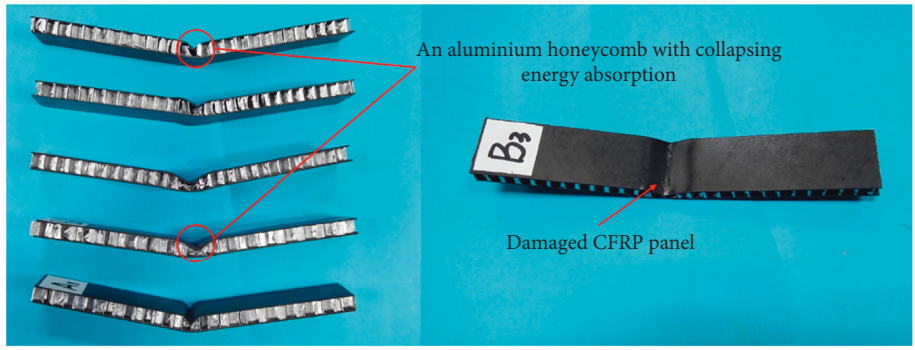

Figure 8: Damaged specimens after quasistatic bending.

under the same testing conditions. In addition, in order to analyze the effect of loading velocity on the crashworthiness of sandwich panels, the loading experiments are carried out at different loading rates for Case E4, Case E5, and Case E6, respectively, and the specimens of Case E4, Case E5, and Case E6 are shown in Figure 6.

4.2. Quasistatic Three-Point Bending Test. The quasistatic three-point bending tests are carried out to study the bending behaviours of these different sandwich panels. All the tests are performed at room temperature in the electronic universal testing machine DNS-100 with a loading capacity of 100 kN. As shown in Figure 7, the speed of the loading roller is from 5 mm/min to 30 mm/min. When the specimens of three groups are tested, the loading velocity of the loading roller is set as 5 mm/min.

In order to analyze the effect of loading velocity on the crashworthiness of sandwich panels, the quasistatic loading test of the specimens of Case E4, Case E5, and Case E6 is carried out, and the loading rates are 5 mm/min, 15 mm/min, and 30 mm/min, respectively. The final bending displacement is set as 25 mm to ensure complete damage for each specimen. The bending load and its corresponding displacement are recorded by a data acquisition system, where the load-displacement curves can be plotted by the system. The deformation behaviours of the specimens are photographed during the quasistatic bending process. The specimens after quasistatic bending failure are shown in Figure 8.

5. Results and Discussion

5.1. Load-Displacement Curves. The load-displacement curves of the sandwich panels with aluminium honeycomb core and CFRP skins under the three-point bending test are shown in Figure 9. The curves can be divided into two stages, namely, the initial elastic bending stage and bending collapse stage [23]. Taking the specimens of Case D (D1, D2, and D3) as an example, in the initial elastic bending stage, the bending load kept increasing until it reaches the first peak (the average value is 435 KN). Following the first peak, extensive microfracture was observed at the corner of the upper panel in contact with the loading roller; the fracture spread quickly in a direction perpendicular to the CFRP skin, causing several drops in the bending load curve within the bending collapse stage as shown in Figure 9; and the numerically predicted peak load matched the experimental measurement with as small error given except for the specimen of Case D1. It is seen that the duration of the elastic deformation stage is very short and the collapse stage is the main energy absorption stage during the bending.

5.2. Failure Modes. The failure progress of the sandwich panels with aluminium honeycomb core and CFRP skins subjected to three-point bending is shown in Figure 10. It shows a complex failure mode, including the plastic hinges, buckling, indentation, core failure, and shear interaction. It is evident that the microfracture initiated at the corner of the top wall in contact with the loading roller

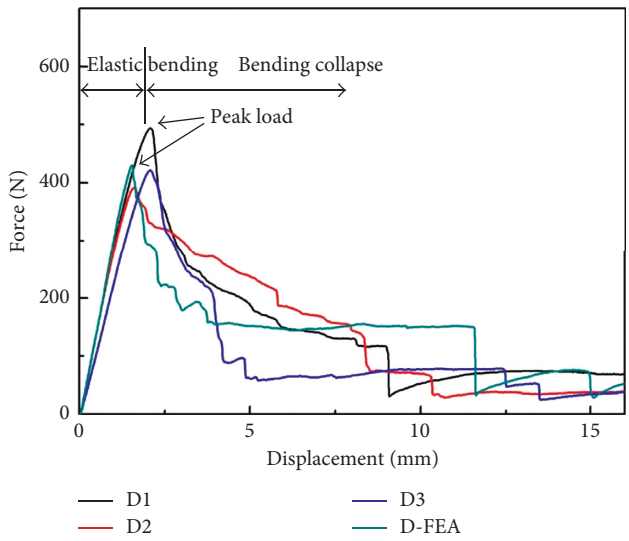

Figure 9: Typical load-displacement curves of specimens in three-point bending tests.

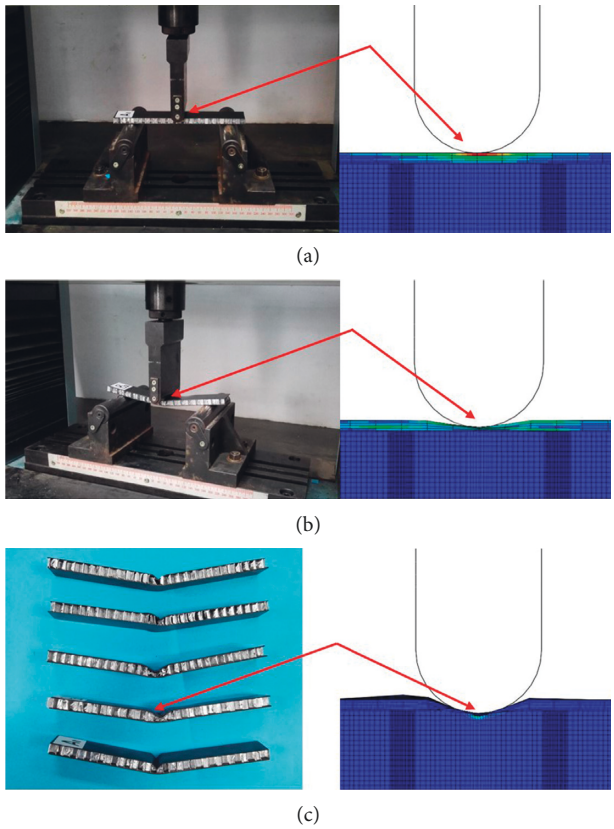

Figure 10: The failure process of sandwich panels in three-point bending tests.

because of the stress concentration. The cracks spread from the top wall of the filled CFRP panels to the aluminium honeycomb. In the bending process, the hexagonal cell layers of aluminium honeycomb are squeezed each other on the upper surface (compression surface) and the cell layers stretched on the bottom surface (tensile surface), leading to a fan shape. But the bending deformation was not enough to induce the cells of the aluminium honeycomb debonding from the adjacent adhesive layers. Therefore, the damage of degumming between aluminium honeycomb cell layers was not found in these three-point bending tests [23].

Table 4: Different fibre directions for FEA and experimental results.

Case	m (g)	F_{max} (N)	F_{avg} (N)	CFE	EA (J)	SEA (J/g)
A1-specimen	22	316	145.7	0.46	3.06	0.14
A2-specimen	20	260	117.1	0.45	2.46	0.12
A3-specimen	20	301	130	0.43	2.73	0.14
A-average	**20.7**	**292.3**	**131**	**0.45**	**2.75**	**0.14**
A-FEA	19.8	300	120	0.40	2.8	0.14
B1-specimen	23	536.7	192.4	0.36	4.81	0.21
B2-specimen	23	525.7	257.6	0.49	6.44	0.28
B3-specimen	23	480.4	231.6	0.48	5.79	0.25
B-average	**23**	**514.3**	**227.2**	**0.44**	**5.68**	**0.25**
B-FEA	19.8	530	245	0.46	5.98	0.30
C1-specimen	23	504	110	0.22	2.75	0.12
C2-specimen	23	533.3	126	0.24	3.15	0.14
C3-specimen	23	481.4	127.2	0.26	3.18	0.14
C-average	**23**	**506.2**	**121**	**0.24**	**3.03**	**0.13**
C-FEA	19.8	527.2	127	0.24	3.1	0.16
D1-specimen	22	492.7	115	0.23	2.99	0.14
D2-specimen	22	389.6	108.8	0.28	2.83	0.13
D3-specimen	22	421.2	87.3	0.21	2.27	0.10
D-average	**22**	**434.5**	**103.7**	**0.24**	**2.7**	**0.12**
D-FEA	19.8	430.7	97.7	0.23	2.54	0.13
E1-specimen	22	341	120.8	0.35	3.14	0.14
E2-specimen	23	372.8	108.8	0.29	2.83	0.12
E3-specimen	23	407.7	85.4	0.21	2.22	0.10
E-average	**22.7**	**373.8**	**105**	**0.28**	**2.73**	**0.12**
E-FEA	19.8	362	120	0.33	3	0.15

5.3. Effect of Fibre Direction on Crashworthiness. The FEA and experimental results of about five kinds of cases (Case A, Case B, Case C, Case D, and Case E) with different fibre directions are listed in Table 4. It indicates that Case A with ±45° fibre direction has the lowest F_{max} (the average value is 294.2 N). On the contrary, Case C with ±60° fibre direction has the highest F_{max} (the average value is 511.5 N). The average value of F_{max} of Case B with ±30° fibre direction is 385.5 N. In addition, the value of F_{avg} of Case B is the highest in these cases. The comparison of CFE of these five different cases is shown in Table 4, and both the CFEs of Case A and Case B are the highest in these cases, indicating that they have the smoothest loading-displacement process. The CFE of these cases are in a range from 0.21 to 0.49 as listed in Table 4. The SEA and EA of these cases are also listed in Table 4. It can be observed that both the SEA and EA of Case B are much higher than those of the other cases, indicating better crashworthiness performance. Except for Case B, both the SEA and EA of Case A are close to those of other cases.

From the above study, the crashworthiness of sandwich panels with aluminium honeycomb core and CFRP skins can be affected by fibre direction. These FEA and experimental results revealed that Case A with ±45° fibre direction has the

Table 5: The deviation values of the experimental results for different fibre directions.

Case	F_{max} error (%)	F_{avg} error (%)	CFE error (%)	EA error (%)	SEA error (%)
A1-specimen	6.3	8.1	11.2	2.2	11.3
A2-specimen	3.4	11	10.6	0	10.5
A3-specimen	3.4	2.9	0.7	4.4	0.7
A-average	**4.4**	**7.3**	**7.5**	**2.2**	**7.5**
B1-specimen	4.4	15.3	18.2	15.3	16
B2-specimen	2.2	13.4	11.4	13.4	12
B3-specimen	6.6	1.9	9	1.9	0
B-average	**4.4**	**10.2**	**12.9**	**10.2**	**9.3**
C1-specimen	0.4	9	8.3	9.2	7.6
C2-specimen	5.4	4.1	0	4	7.7
C3-specimen	4.9	5.1	8.3	4.9	7.7
C-average	**3.6**	**6.1**	**5.5**	**6.0**	**7.7**
D1-specimen	13.4	10.9	4.2	10.7	16.7
D2-specimen	10.3	4.9	16.7	4.8	8.3
D3-specimen	3	15.8	12.5	15.9	16.7
D-average	**8.9**	**10.5**	**11.1**	**10.5**	**13.9**
E1-specimen	8.8	15	25	15	16.7
E2-specimen	0.3	3.6	35.7	3.6	0
E3-specimen	9	18.7	25	18.7	16.7
E-average	**6.0**	**12.4**	**28.6**	**12.4**	**11.1**

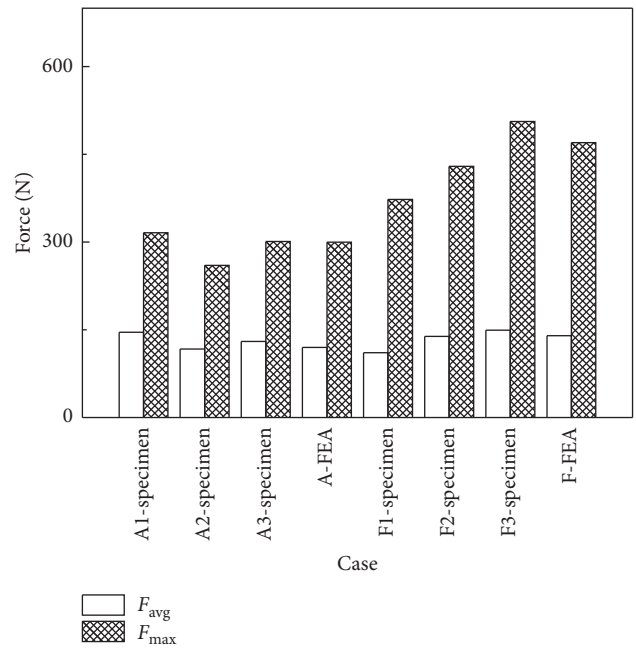

Figure 11: Comparison of different stacking sequence for specimens: F_{max} and F_{avg}.

lowest F_{max}, but not the highest EA and SEA. In addition, Case B with ±30° fibre direction has the highest EA and SEA, but not the lowest F_{max}. The lowest F_{max}, highest EA, and highest SEA indicate better crashworthiness performance. Summarizing the respective advantages of fibre direction of ±30° and ±45°, both of these fibre directions should be considered in the ply design. The deviation values of the experimental results for different fibre directions are shown in Table 5. It is found that the deviation values are less than 10%. Therefore, the results of the experimental results for different fibre directions are reliable. It is noted that because the values of CFE are very small, it will lead to a large deviation in calculations.

5.4. Effect of Stacking Sequence on Crashworthiness. Case A and Case F are considered to analyze the effect of stacking sequence on crashworthiness performance. The comparison of F_{max} and F_{avg} of the two cases is shown in Figure 11. It indicates that the F_{max} of Case A is lower than that of Case F. The F_{avg} of Case A is close to that of Case F. As shown in Figure 12, the CFE of Case A is higher than that of Case F, indicating that Case A has the smoother loading-displacement process. The SEA and EA of these two cases are shown in Figure 13. It can be observed that the SEA and EA of Case A are higher than those of Case F, indicating better crashworthiness performance.

It can be concluded that the crashworthiness of sandwich panels with aluminium honeycomb core and CFRP skins can be affected by the stacking sequence. By comparing both Case A and Case F crashworthiness criteria, the results reveal that Case A with an asymmetrical stacking sequence design has better crashworthiness performance.

5.5. Effect of Layer Thickness on Crashworthiness. As shown in Table 6, there are three kinds of cases (Case A, Case G, and Case H) with different layer thicknesses. For Case A, the layer thickness is 0.8 mm; for Case G, the layer thickness is 0.6 mm; and for Case H, the layer thickness is 0.4 mm. With the increase in the layer thickness, both the F_{avg} and CFE increase. Interestingly, the F_{max} is approximately the same. With the increase in the layers thickness, both the EA and SEA increase. Both the EA and SEA of Case A are the highest of these three kinds of cases. Therefore, in general, with increase in the layer thickness, the sandwich panels with aluminium honeycomb core and CFRP skins would have higher energy absorption capacities. The deviation values of the experimental results for different layer thicknesses are shown in Table 7. It was found that the deviation values are less than 10%. Therefore, the experimental results for different fibre directions are reliable.

5.6. Effect of Loading Velocity on Crashworthiness. To investigate the effect of loading velocity on the crashworthiness of sandwich panels with aluminium honeycomb core and CFRP skins, the load-displacement curves of specimens (Case E4, Case E5, and Case E6) with different velocities are plotted in Figure 14. With the increase in the loading velocity, the F_{max} of specimens of Case E increases. When the loading velocity is 30 mm/min, the F_{max} of the specimen of Case E6 is the highest.

The comparison of CFE of three specimens (Case E4, Case E5, and Case E6) with different loading velocities is graphed in Figure 15, and the F_{max} and F_{avg} are also graphed in Figure 15. The CFE of the specimen of Case E5 with minimum loading velocity is the highest.

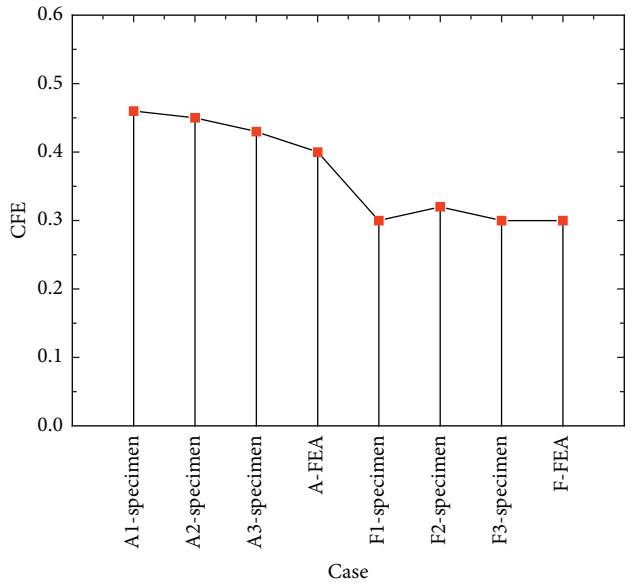

Figure 12: Comparison of different stacking sequence for specimens: CFE.

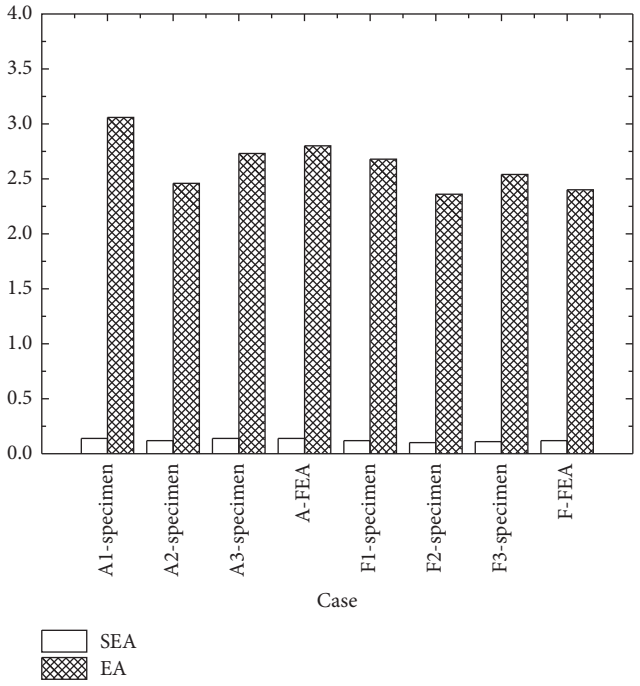

Figure 13: Comparison of different stacking sequence for specimens: EA and SEA.

The EA and SEA of three specimens (Case E4, Case E5, and Case E6) are graphed in Figure 16. It can be observed that the EA and SEA of the specimen of Case E5 with minimum loading velocity are much higher than those of other specimens.

It can be concluded the crashworthiness of sandwich panels with aluminium honeycomb core and CFRP skins can be affected by loading velocity. By comparing the crashworthiness criteria, the results reveal that the specimen of

Table 6: Different layer thicknesses for FEA and experimental results.

Case	m (g)	F_{max} (N)	F_{avg} (N)	CFE	EA (J)	SEA (J/g)
A1-specimen	22	316	145.7	0.46	3.06	0.14
A2-specimen	20	260	117.1	0.45	2.46	0.12
A3-specimen	20	301	130	0.43	2.73	0.14
A-average	**20.7**	**292.3**	**131**	**0.45**	**2.75**	**0.14**
A-FEA	19.8	300	120	0.40	2.8	0.14
G1-specimen	23	329.6	88.7	0.27	1.33	0.06
G2-specimen	22	360.8	100.6	0.28	1.51	0.07
G3-specimen	22	351	94	0.27	1.41	0.06
G-average	**22.3**	**347.1**	**94.4**	**0.27**	**1.41**	**0.06**
G-FEA	15.5	328	90	0.27	1.38	0.09
H1-specimen	16	316.6	69.3	0.22	1.04	0.07
H2-specimen	16	282.2	84	0.30	1.26	0.08
H3-specimen	16	301.9	80.7	0.27	1.21	0.08
H-average	**16**	**300.2**	**78**	**0.26**	**1.17**	**0.08**
H-FEA	11.3	300	77	0.26	1.1	0.10

Table 7: The deviation values of the experimental results for layer thicknesses.

Case	F_{max} error (%)	F_{avg} error (%)	CFE error (%)	EA error (%)	SEA error (%)
A1-specimen	6.3	8.1	11.2	2.2	11.3
A2-specimen	3.4	11	10.6	0	10.5
A3-specimen	3.4	2.9	0.7	4.4	0.7
A-average	**4.4**	**7.3**	**7.5**	**2.2**	**7.5**
G1-specimen	5	6	0	5.7	0
G2-specimen	3.9	6.6	3.7	7.1	16.7
G3-specimen	11.2	0.4	0	0	0
G-average	**6.7**	**4.3**	**1.2**	**4.3**	**5.6**
H1-specimen	5.5	11	15.4	11	12.5
H2-specimen	6	7.7	15.4	7.7	0
H3-specimen	5.7	3.5	3.8	3.4	0
H-average	**5.7**	**7.4**	**11.5**	**7.4**	**4.2**

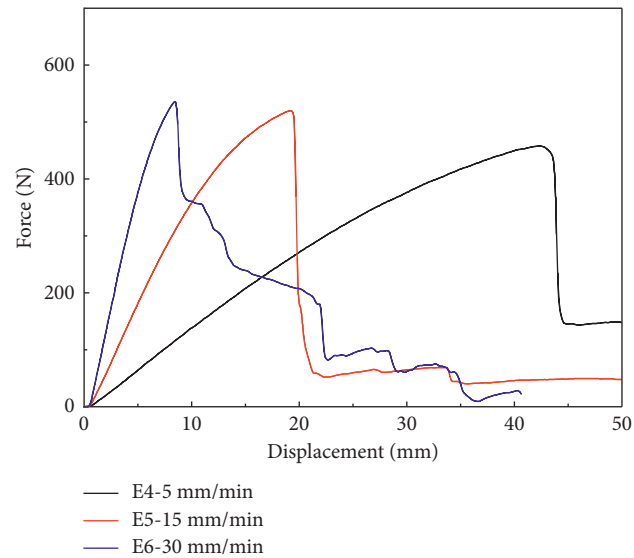

Figure 14: Load-displacement curves of specimens with different velocities on crashworthiness.

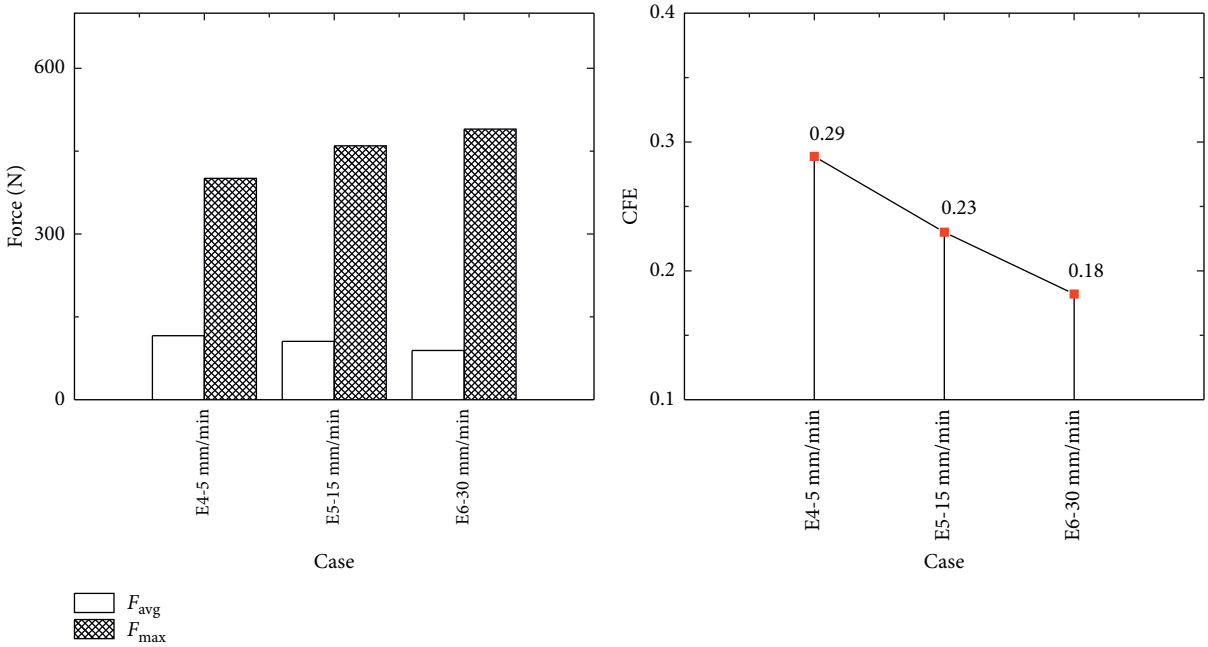

Figure 15: Comparison of different loading velocities for specimens: F_{max}, F_{avg}, and CFE.

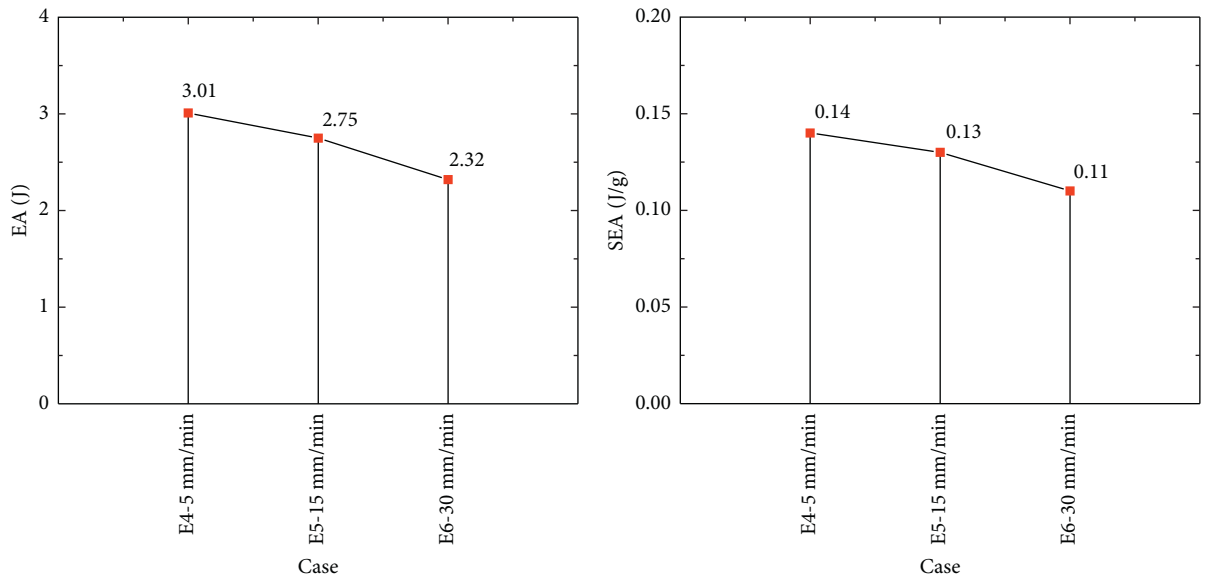

Figure 16: Comparison of different loading velocities for specimens: EA and SEA.

Case E5 with minimum loading velocity has the best crashworthiness performance.

6. Conclusions

This study presented a numerical and experimental study on bending responses of sandwich panels with aluminium honeycomb core and CFRP skins under quasistatic bending load. The typical load-displacement curves, failure modes, and energy absorption are explored. Within the limitation of the study, the following conclusions can be drawn:

(1) The load-displacement curves of the sandwich panels with aluminium honeycomb core and CFRP skins under the three-point bending test can be divided into the initial elastic bending stage and bending collapse stage. The sandwich panels with aluminium honeycomb core and CFRP skins absorbed most of the energy during bending collapse stage.

(2) The FEA prediction and experiment are used in understanding the initiation and propagation of cracks within the sandwich panels with aluminium honeycomb core and CFRP skins. The microfracture initiates at the corner of the top wall in contact with the loading roller. The cracks spread from the top wall of the filled CFRP skins to the aluminium honeycomb. In the bending process, the hexagonal cell layers of

aluminium honeycomb are squeezed each other, leading to a fan shape. But the bending deformation was not enough to induce the cells of the aluminium honeycomb debonding from the adjacent adhesive layers.

(3) The crashworthiness of sandwich panels with aluminium honeycomb core and CFRP skins can be affected by fibre direction. Case A with ±45° fibre direction has the lowest F_{max}, but not the highest EA and SEA. In addition, Case B with ±30° fibre direction has the highest EA and SEA, but not the lowest F_{max}. Therefore, both of these fibre directions should be considered in the ply design.

(4) The crashworthiness of sandwich panels with aluminium honeycomb core and CFRP skins can be affected by the stacking sequence. By comparing both Case A and Case F crashworthiness criteria, the results reveal that Case A with symmetrical ply design has a better crashworthiness performance.

(5) In general, with the increase in the layer thickness, the sandwich panels with aluminium honeycomb core and CFRP skins would have higher energy absorption capacities. The crashworthiness of sandwich panels can be affected by loading velocity. The experimental results reveal that the specimen of Case E5 with minimum loading velocity (5 mm/min) has the best crashworthiness performance.

In summary, this study demonstrates the potential of sandwich panels with aluminium honeycomb core and CFRP skins to be an energy absorber used in electric vehicle body; and the experimental results can also be used for validating the numerical simulation for design optimization of the sandwich panels with aluminium honeycomb core and CFRP skins in the future.

Data Availability

The data used to support the findings of this study have been included within the article.

Conflicts of Interest

The authors declare that there are no conflicts of interest regarding the publication of this paper.

Acknowledgments

This work was supported by the National Natural Science Foundation of China-China Aerospace Science and Technology Corporation joint fund of aerospace advanced manufacturing technology research (no. U1537103), the Fundamental Research Funds for the Central Universities (WUT: 2017III047), and the Fundamental Research Funds for the Central Universities (WUT: 2018IVA023).

References

[1] Q. Liu, Z. Ou, Z. Mo, Q. Li, and D. Qu, "Experimental investigation into dynamic axial impact responses of double hat shaped CFRP tubes," *Composites Part B: Engineering*, vol. 79, pp. 494–504, 2015.

[2] Q. Liu, Z. Mo, Y. Wu, J. Ma, G. C. P. Tsui, and D. Hui, "Crush response of CFRP square tube filled with aluminum honeycomb," *Composites Part B: Engineering*, vol. 98, pp. 406–414, 2016.

[3] Q. Liu, J. Ma, X. Xu, Y. Wu, and Q. Li, "Load bearing and failure characteristics of perforated square CFRP tubes under axial crushing," *Composite Structures*, vol. 160, pp. 23–35, 2017.

[4] S. Hou, S. Zhao, L. Ren, X. Han, and Q. Li, "Crashworthiness optimization of corrugated sandwich panels," *Materials and Design*, vol. 51, pp. 1071–1084, 2013.

[5] O. T. Thomsen and W. M. Banks, "An improved model for the prediction of intra-cell buckling in CFRP sandwich panels under in-plane compressive loading," *Composite Structures*, vol. 65, no. 3-4, pp. 259–268, 2004.

[6] S. Shi, Z. Sun, X. Hu, and H. Chen, "Flexural strength and energy absorption of carbon-fiber–aluminum-honeycomb composite sandwich reinforced by aluminum grid," *Thin-Walled Structures*, vol. 84, pp. 416–422, 2014.

[7] I. Ivañez and S. Sanchez-Saez, "Numerical modelling of the low-velocity impact response of composite sandwich beams with honeycomb core," *Composite Structures*, vol. 106, no. 12, pp. 716–723, 2013.

[8] Y. Wu, Q. Liu, J. Fu, Q. Li, and D. Hui, "Dynamic crash responses of bio-inspired aluminum honeycomb sandwich structures with CFRP panels," *Composites Part B: Engineering*, vol. 121, pp. 122–133, 2017.

[9] M. Paulino, F. Teixeira Dias, C. P. Gameiro, and J. Cirne, "Hyperelastic and dynamical behaviour of cork and its performance in energy absorption devices and crashworthiness applications," *International Journal of Materials Engineering Innovation*, vol. 1, no. 2, p. 197, 2009.

[10] R. D. Hussein, D. Ruan, and J. W. Yoon, "An experimental study of square aluminium tubes with honeycomb core subjected to quasi-static compressive loads," *Key Engineering Materials*, vol. 626, pp. 91–96, 2015.

[11] Y. Zhang, Z. Zong, Q. Liu, J. Ma, Y. Wu, and Q. Li, "Static and dynamic crushing responses of CFRP sandwich panels filled with different reinforced materials," *Materials and Design*, vol. 117, pp. 396–408, 2017.

[12] N. Tomizawa, T. Tsujimoto, K. Itoh, T. Ogino, K. Nakamura, and S. Hara, "Numerical and experimental study of crashworthiness parameters of honeycomb structures," *Thin-Walled Structures*, vol. 78, no. 4, pp. 87–94, 2014.

[13] A. Ashab, R. Dong, G. Lu, and Y. C. Wong, "Quasi-static and dynamic experiments of aluminum honeycombs under combined compression-shear loading," *Materials and Design*, vol. 97, pp. 183–194, 2016.

[14] X. Zhang, H. Zhang, and Z. Wen, "Experimental and numerical studies on the crush resistance of aluminum honeycombs with various cell configurations," *International Journal of Impact Engineering*, vol. 66, pp. 48–59, 2014.

[15] K. B. Shin, J. Y. Lee, and S. H. Cho, "An experimental study of low-velocity impact responses of sandwich panels for Korean low floor bus," *Composite Structures*, vol. 84, no. 3, pp. 228–240, 2008.

[16] C. C. Foo, G. B. Chai, and L. K. Seah, "Quasi-static, and low-velocity impact, failure of aluminium honeycomb sandwich panels," *Proceedings of the Institution of Mechanical Engineers Part L: Journal of Materials: Design and Applications*, vol. 220, no. 2, pp. 53–66, 2006.

[17] G. Sun, X. Huo, D. Chen, and Q. Li, "Experimental and numerical study on honeycomb sandwich panels under bending and in-panel compression," *Materials and Design*, vol. 133, pp. 154–168, 2017.

[18] G. Sun, S. Li, Q. Liu, G. Li, and Q. Li, "Experimental study on crashworthiness of empty/aluminum foam/honeycomb–filled CFRP tubes," *Composite Structures*, vol. 152, pp. 969–993, 2016.

[19] M. A. Hazizan and W. J. Cantwell, "The low velocity impact response of an aluminium honeycomb sandwich structure," *Composites Part B: Engineering*, vol. 34, no. 8, pp. 679–687, 2003.

[20] V. Crupi, E. Kara, G. Epasto, E. Guglielmino, and H. Aykul, "Theoretical and experimental analysis for the impact response of glass fibre reinforced aluminium honeycomb sandwiches," *Journal of Sandwich Structures and Materials*, vol. 20, no. 1, pp. 42–69, 2016.

[21] R. D. Hussein, R. Dong, G. Lu, and I. Sbarski, "Axial crushing behaviour of honeycomb-filled square carbon fibre reinforced plastic (CFRP) tubes," *Composite Structures*, vol. 140, pp. 166–179, 2016.

[22] J. C. Liu and H. C. Wu, "Fiber direction and stacking sequence design for bicycle frame made of carbon/epoxy composite laminate," *Materials and Design*, vol. 31, no. 4, pp. 1971–1980, 2010.

[23] Q. Liu, X. Xu, J. Ma, J. Wang, Y. Shi, and D. Hui, "Lateral crushing and bending responses of CFRP square tube filled with aluminum honeycomb," *Composites Part B: Engineering*, vol. 118, pp. 104–115, 2017.


The Scientific
World Journal
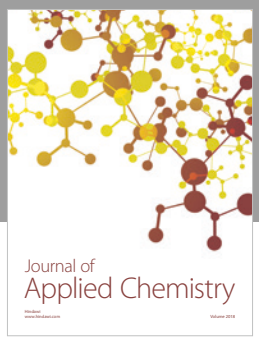
Journal of
Applied Chemistry
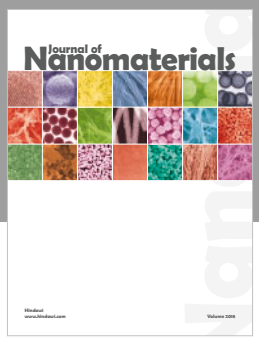
Journal of
Nanomaterials

Scientifica

International Journal of
Polymer Science
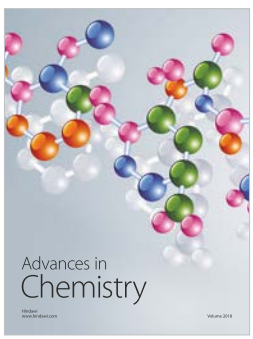
Advances in
Chemistry

Hindawi
Submit your manuscripts at
www.hindawi.com
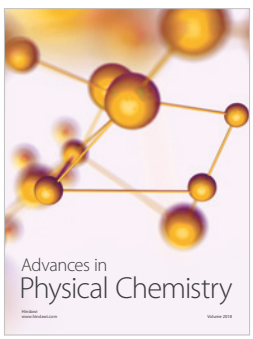
Advances in
Physical Chemistry

International Journal of
Analytical Chemistry
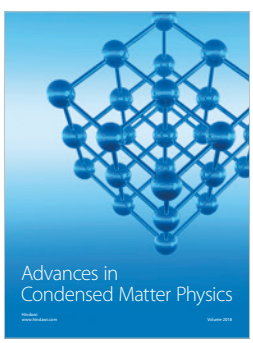
Advances in
Condensed Matter Physics
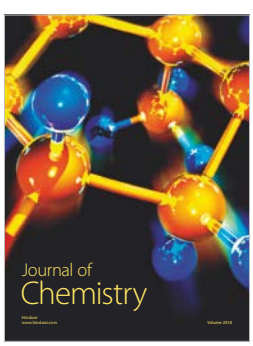
Journal of
Chemistry

International Journal of
Biomaterials
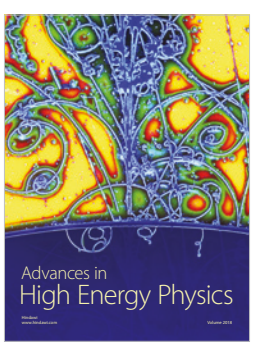
Advances in
High Energy Physics

Journal of
Engineering

Journal of
Nanotechnology

International Journal of
Corrosion

Journal of
Materials

BioMed
Research International
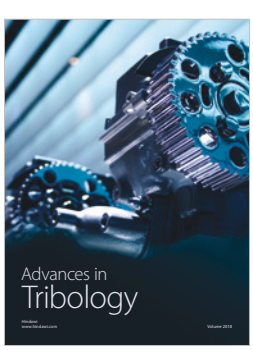
Advances in
Tribology
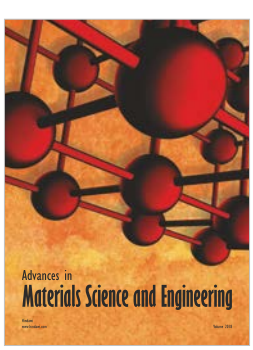
Advances in
Materials Science and Engineering